Bioresorbable optical fiber Bragg gratings

Bioresorbable optical fiber Bragg gratings

DIEGO PUGLIESE,[1] MARIA KONSTANTAKI,[2,*] IOANNIS KONIDAKIS,[2] EDOARDO CECI-GINISTRELLI,[1] NADIA G. BOETTI,[3] DANIEL MILANESE,[1,4] AND STAVROS PISSADAKIS[2]

[1]*Dipartimento di Scienza Applicata e Tecnologia and INSTM, Politecnico di Torino, Corso Duca degli Abruzzi 24, 10129 Torino, Italy*
[2]*Institute of Electronic Structure and Laser (IESL), Foundation for Research and Technology - Hellas (FORTH), 100 N. Plastira Street, Vassilika Vouton, 70013 Heraklion, Crete, Greece*
[3]*Istituto Superiore Mario Boella, Via P. C. Boggio 61, 10134 Torino, Italy*
[4]*IFN - CNR, CSMFO Lab., Via alla Cascata 56/C, 38123 Povo, TN, Italy*
**Corresponding author: mkonst@iesl.forth.gr*

Received XX Month XXXX; revised XX Month, XXXX; accepted XX Month XXXX; posted XX Month XXXX (Doc. ID XXXXX); published XX Month XXXX

We demonstrate for the first time inscription and wet dissolution study of Bragg gratings in a bioresorbable calcium-phosphate glass optical fiber. Bragg gratings, with average refractive index changes of 5.8 x 10^{-4}, were inscribed using 193 nm excimer laser radiation. Results on the dissolution of the irradiated fiber in simulated physiological conditions are presented after immersing a tilted Bragg grating in phosphate buffered saline solution for 56 h selective chemical etching effects are also reported. The investigations performed pave the way towards the use of such phosphate glass fiber Bragg gratings for the development of soluble photonic sensing probes for the efficient in-vivo monitoring of vital mechanical or chemical parameters.

OCIS codes: *(060.3735) Fiber Bragg gratings; (060.3738) Fiber Bragg gratings, photosensitivity; (060.2370) Fiber optics sensors; (160.2290) Fiber materials; (160.1435) Biomaterials.*

http://dx.doi.org/10.1364/OL.99.099999

During the last two decades, optical fiber technology has achieved increasing penetration in biomedicine [1] with indicative applications in endoscopic imaging, localized tissue modification and diagnostic and therapeutic sensing [2]. Focusing on biomedical sensing, there are applications where a glass optical fiber should be attached or even inserted inside the human body for obtaining information. A critical requirement which arises with respect to such a sensor is that of biocompatibility; a condition that is intrinsically satisfied by conventional silica optical fibers, which are nontoxic and biochemically inert. However, silica is a hard and chemically resistant glass, thus an accidental breakage is dangerous for the patient, rendering this choice non-preferable for interstitial or intravascular uses. The solution to this problem can be represented by a bioresorbable glass; a glass that can be safely assimilated by the human body in a limited amount of time in case of breakage.

The requirement for soluble sensors in medical applications is widely recognized among relevant communities and recent studies have also been presented involving additional technologies such as bioresorbable silicon electronic sensors [3]. For the case of biocompatible and resorbable optical fibers, noticeable research efforts in the last decades have led to the fabrication of biodegradable fibers and waveguides for sensing purposes employing glasses but also polymers and silk based materials [4-9]. However, for sensing applications the fiber must exhibit good mechanical durability, high optical transmission and a stoichiometrically tunable dissolution rate. With this aim, studies employing phosphate glasses have recently resulted in the fabrication of optical fibers with enhanced optical transmission properties, allowing the drastic reduction of optical propagation loss [9]. These magnesium-calcium-phosphate glass fibers contain non-toxic ion-modifiers that define their chemical and optical properties and dissolve in simulated physiological conditions e.g. in Phosphate Buffered Saline (PBS) solution [9].

One of the most promising technologies that has been suggested for biomedical sensing applications involving optical fibers is that of Fiber Bragg Gratings (FBGs) [10, 11]. FBG sensors are a mature photonic technology with established applications in structural health monitoring, while their use in a wide selection of biosensing applications has also been suggested including articular joint pressure monitoring [12], plantar pressure and human–machine interface sensing pads [13], DNA detection [14] and measuring of mechanical strain in bones [15].

Herein we demonstrate the first inscription of Bragg gratings in a bioresorbable phosphate glass optical fiber. Initially, we report on the inscription of standard and tilted Bragg gratings. Subsequently, the tilted Bragg gratings are used for spectrally monitoring the dissolution of the optical fiber in PBS solution, with pH and temperature conditions that resemble those of the human body. Scanning electron microscopy (SEM) analysis of the dissolved optical fibers revealed that selective chemical etching occurs and strongly depends on the intensity of the inscription laser beam absorbed by the fiber. Finally, a Raman study is also presented to further examine the effect of UV irradiation on the glass fiber.

While the inscription of Bragg gratings in phosphate and phosphosilicate glass optical fibers has been demonstrated [16] in the past using deep ultraviolet (193 nm) laser radiation [17, 18], the present study investigates how Bragg gratings inscribed in bioresorbable optical fibers behave under controlled dissolution conditions, for projecting possible intra-vein/-body applications and possible hurdles that may arise towards this direction.

The bioresorbable optical fiber employed for the grating inscriptions was fabricated by preform drawing, with the preform being obtained by the rod-in-tube technique. The core and cladding glasses were synthesized by melting a powder batch of high purity (99+%) chemicals (P_2O_5, CaO, MgO, Na_2O, B_2O_3, SiO_2) inside an alumina crucible at a temperature of 1200 °C for 1 h, followed by casting into preheated brass molds. The core glass was cast into a cylindrical mold to form a 12 mm diameter rod, while two identical cladding tubes were shaped by rotational casting at a rotation speed of 3000 rpm using an equipment developed in-house. The core and cladding calcium-phosphate glass compositions were *ad-hoc* engineered to guarantee a unique combination of optical and biological functionalities [9]. In particular, the glasses resulted to be: homogeneous; stable against de-vitrification (ΔT ~ 200 °C) and therefore suitable for fiber drawing; soluble in simulated physiological conditions (PBS, pH = 7.4 at 37 °C) with a dissolution rate of 2-4 μm/day; transparent in the near UV region down to 240 nm. The transparency in the near UV region represents one of the most important assets of glass based biocompatible and resorbable optical fibers with respect to polymer based bioresorbable waveguides [19], and is a feature of paramount importance in view of introducing significant changes in the refractive index of the material by appropriate UV irradiation. The optical fiber showed diameters of 15 and 120 μm for the core and the cladding, respectively, with a corresponding numerical aperture (NA) value of 0.07. These parameters were designed in order to achieve a single-mode behavior at 1550 nm, while an attenuation loss of 1.9 dB/m at 1300 nm was measured by the cut-back technique.

For the inscription of the Bragg gratings, a standard 1064.7 nm period phase mask setup, with a 193 nm high spatial coherence and 10 ns pulse duration excimer laser (Braggstar, TUI laser), was used. The energy density of the inscription beam was set to 108 mJ/cm^2, as higher energy densities were found to induce surface damage to the fiber cladding. The gratings transmission and reflection spectra were monitored in real time during inscription using a broadband superluminescent diode source and an optical spectrum analyzer, while a length of phosphate fiber (typically of the order of 10 cm) was fusion spliced to standard single-mode fiber (SMF28e, Corning Inc.). Typical losses per splice were of the order of 1 dB, at 1550 nm. A 100 min irradiation at 10 Hz resulted in the monotonous shift of the inscribed Bragg wavelength to higher values before reaching saturation. A 6 dB strong notch was formed for an accumulated energy density dose of approximately 4 J/cm^2 (see Fig. 1(a)). This grating inscription behavior is considered to be of Type I [16]. Based on the Bragg wavelength shift measured, the induced average refractive index change at the end of the inscription is equal to 5.8 x 10^{-4} [10].

The cladding mode resonances observed in optical fiber Bragg gratings are an efficient way to monitor surface related phenomena, rendering them suitable for studying the dissolution of the phosphate glass optical fiber. However, the phosphate glasses constituting the core and cladding of this optical fiber have almost the same stoichiometry. Therefore, grating fringes are written in both glasses and as a result coupling to cladding modes, typically observed for standard Bragg gratings, is suppressed [20]. The cladding mode coupling suppression is facilitated by modal orthogonality. This condition is automatically satisfied for refractive index modulations uniformly recorded over the whole area of the fiber cross-section and renders the coupling constant overlap equal to zero. To overcome this inherent photosensitivity issue, tilted Bragg gratings [21] were recorded to excite cladding modes of azimuthal parity.

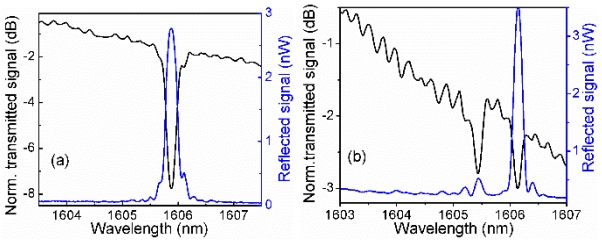

Fig. 1. Normalized transmission (black in online color edition) and reflection (blue in online color edition) signals of (a) a standard FBG after accumulated energy density dose of 4 J/cm^2 and (b) a FBG with a 1° tilt angle and accumulated energy density dose of 5.2 J/cm^2; for both inscriptions the UV laser beam pulse energy density was 108 mJ/cm^2 and the repetition rate 10 Hz.

Attempts to inscribe tilted FBGs with the conditions described above and a tilting angle of 2° did not result in measurable Bragg and cladding mode resonance signals, thus the tilting angle was lowered to 1°. Fig. 1(b) shows the normalized 1° tilted FBG transmission and reflection signals for an accumulated energy density dose of 5.2 J/cm^2. The increased inscription energy dose, compared to that used for the standard gratings, was required in order to inscribe strong cladding mode resonances. In addition to the fundamental Bragg peak attenuation signal, that is diminished in strength in comparison to the standard inscription but still present at 1606 nm, the tilted FBG spectra exhibit the so-called "ghost" peak at 1605.3 nm. This peak has similar characteristics with the Bragg line and is attributed to the superposition of several tightly confined lower order cladding modes [22]. The phosphate fiber–SMF splice joints may induce back reflection of light [23] and core-cladding coupling, which can lead to multimodal interference spectral fringes due to the small length of the spliced fiber. As a result, the small cladding mode resonances at lower wavelengths are masked in the transmission signal, while in the reflected signal a few weak cladding mode peaks are visible.

To allow online monitoring of the optical fiber dissolution, the tilted FBG was immersed into PBS solution, in pH and temperature conditions that resemble those of the human body. The evolution of the grating signal was monitored regularly, starting from the first few minutes after immersion up to 56 h. The spectra recorded for the reflected and transmitted signals are shown in Figs. 2(a) and (b), respectively. It is worthwhile to note that changes in the reflected signal are evident just after a few hours in the solution, with the emerging of additional cladding mode peaks in the region between 1603 and 1605 nm. For prolonged immersion periods (49 h onwards), the fundamental FBG peak is also modified in wavelength, shape and strength. In particular, a strength drop

from an initial value of 0.78 dB down to 0.25 dB was registered after an immersion time of 56 h in PBS.

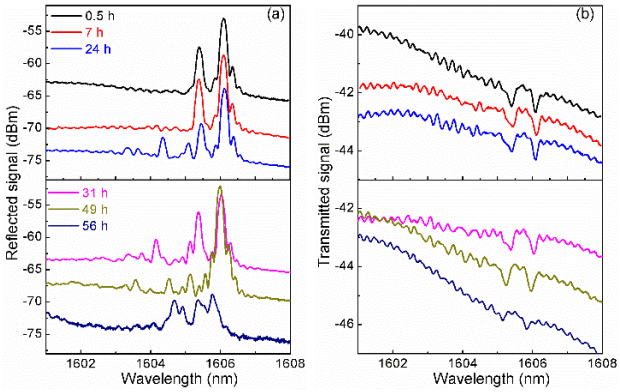

Fig. 2. Reflected (a) and transmitted (b) signals evolution of a 1° tilted FBG immersed in PBS solution for up to 56 h. The baseline of the different spectra has been adjusted vertically to assist visualization.

Similar conclusions are drawn from the transmitted signal spectra, where the similarity in the response of the fundamental and ghost peaks is reinforced. This behavior is not surprising, since the ghost mode corresponds to low order cladding modes characterized by a modal dispersion response which is highly similar to that of the core guiding mode manifested at the fundamental Bragg peak [21]. Nonetheless, this profound change in the signal of the fundamental FBG peak for an immersion time of 56 h was a rather unexpected finding, since previous studies [9] had indicated that the dissolution of the optical fiber with this specific stoichiometry exhibits slower diameter decrease rate of 2-4 μm/day.

To further examine the dissolution process of the exposed optical fiber, SEM images of an optical fiber with a Bragg grating immersed in PBS solution for up to 56 h (see Figs. 3(a) and (b)) were acquired. These SEM images revealed a profound selective chemical etching process induced by the PBS medium; namely, the laser exposed region exhibited a manifold faster dissolution rate, resulting in the sculpting of a relief pattern onto the phosphate glass optical fiber surface. As expected, the faster dissolution rate of the UV exposed phosphate glass regions closely depends on the laser intensity pattern [24].

In order to gain additional information on the dependence of the etching rate on the intensity distribution of the irradiating laser beam within the fiber volume, a phosphate glass optical fiber with a Bragg reflector, inscribed with the aforementioned conditions, was cleaved within the FBG section and the exposed fiber was subsequently immersed in the PBS solution for 5 h. Fig. 3(c) shows a SEM image of the end face of the optical fiber, revealing a non-circularly symmetric dissolved pattern closely following the caustic intensity of the irradiation beam. This experimental finding confirms previous finite difference time domain (FDTD) simulations (OptiFDTD) of the propagation of the externally side-illuminated laser beam for Bragg grating recording, wherein the cladding interface causes beam lensing inside the optical fiber volume as shown in Fig. 3(d) [25]. The agreement between the experimental and the simulation results of Figs. 3(c) and (d) is particularly prominent. The laser assisted selective chemical etching in a non-toxic solution demonstrated for this bioresorbable glass optical fiber can pave the way towards the development of optical fiber and planar microfluidic/optofluidic disposable sensing devices.

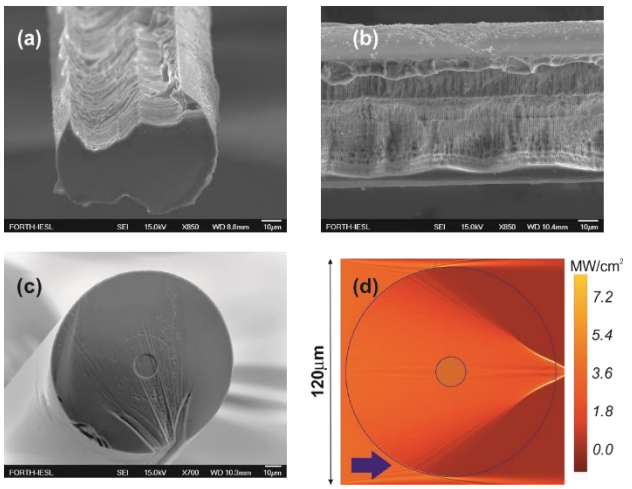

Fig. 3. End face (a) and side (b) views of the cladding region of an irradiated optical fiber (energy dose of 5.2 J/cm^2) immersed in PBS. A side section of the fiber was intentionally removed to reveal inner regions. (c) End face view of the FBG region after 5 h in PBS and (d) FDTD simulation of intensity spatial distribution (input beam intensity 3.6 MW/cm^2) of a side-irradiated optical fiber. The blue arrow in (d) indicates the direction of laser beam illumination.

The asymmetric dissolution of the optical fiber critically affects the evolution of the cladding mode spectral signature (see Fig. 2), rendering its exact theoretical description based on the optical fiber diameter change impossible. This signal evolution due to the selective glass etching, even in the absence of a targeted sensing parameter, depends on the fiber composition, dissolution environment conditions (e.g. pH and temperature) and exposure conditions. For the specific experimental conditions employed, the fundamental Bragg resonance is spectrally unaffected for at least 49 h after the immersion. It is expected that multi-cladding optical fibers of controlled dissolution could be fabricated (by tuning phosphate glass composition) for which the fundamental mode is not largely affected by the wet etching of the fiber cladding during the time span required for a specific application.

Additional experiments were performed as described in detail in [9] for determining the dissolution rate in PBS of the phosphate glass fiber following Bragg grating inscription with a UV energy dose of 5.2 J/cm^2. An etching rate of ~ 20 μm/day was obtained, which is significantly greater than that of the pristine fiber [9]. Previous studies have shown that prolonged exposure of the phosphate glass to radiation with photon energy within the Urbach tail of the material results in extensive de-polymerization of the glass network, mostly prompted by the cleaving of P-O bonds [26, 27]; this radiation induced structural modification can accelerate the wet dissolution process of the exposed glass. Thus, for further investigating the dissolution mechanism of the phosphate fibers in simulated physiological conditions, micro-Raman spectroscopy has been carried out both on pristine and UV exposed fibers before and after immersion in PBS.

Fig. 4 presents the Raman spectra of the fibers before and after UV exposure (radiation dose of 5.2 J/cm^2), as well as the

corresponding spectra of the same fibers after their immersion in PBS solution for 5 h. The UV exposed fiber shows an increase in the intensity of the band at ca. 1180 cm^{-1} corresponding to the symmetric stretching vibration of terminal PO_2^- groups relative to that of P-O-P bridges stretching vibration at ca. 710 cm^{-1} [28, 29], indicating a noticeable de-polymerization of the phosphate glass network upon laser exposure, in agreement with previous reports [26, 27].

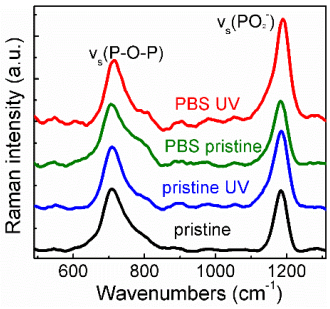

Fig. 4. Raman spectra of the phosphate fibers before and after UV exposure at an UV energy dose of 5.2 J/cm^2 and corresponding spectra after fiber immersion in PBS solution for 5 h. To allow comparison, all spectra are normalized with respect to the band at ca. 710 cm^{-1}.

While the weathering of phosphate glasses within aqueous solutions starts with the hydrolysis of the modifier cations, it eventually continues with the incorporation of hydroxyl (-OH) groups bonded to the phosphate network. The latter process can take place via two mechanisms, namely by either breaking P-O-P bridges for the formation of chain terminating P-OH groups under the reaction scheme P-O-P + $H_2O \rightarrow$ 2 (P-OH), or/and by separating cation chain links under the scheme P-O-M + $H_2O \rightarrow$ P-OH + M-OH, where M is the modifier cation [30]. Raman analysis revealed that the predominant mechanism for the introduction of -OH hydroxyl groups to the UV irradiated fiber is indeed the first, as the irradiated fiber placed in PBS solution exhibits the largest I(PO_2^-)/I(P-O-P) ratio (1.65), thus pointing out that -OH groups are incorporated to the expense of P-O-P bridges. Notably, the corresponding ratio for the pristine fiber immersed in PBS for the same period is considerably lower, i.e. 1.05, highlighting the importance of UV irradiation on the initiating of the hydrolysis process.

In summary, we have shown the inscription of Bragg gratings in a phosphate glass resorbable optical fiber and studied their selective wet dissolution behavior in simulated physiological conditions. The results presented indicate that gratings with tailored dissolution behavior, controlled by fiber composition, inscription conditions and dissolving medium, could be fabricated for in-vivo applications with a specific time span of operation, such as deep-tissue photodynamic therapy including ablation processes [31].

Funding. COST Action MP1401 "Advanced Fibre Laser and Coherent Source as tools for Society, Manufacturing and Lifescience"

Acknowledgment. SP warmly thanks Georgios D. Tsibidis for performing FDTD simulations.

REFERENCES

1. G. Keiser, F. Xiong, Y. Cui, and P. P. Shum, "Review of diverse optical fibers used in biomedical research and clinical practice," J. Biomed. Opt. 19, 080902 (2014).
2. L. C. L. Chin, W. M. Whelan, and I. A. Vitkin, "Optical Fiber Sensors for Biomedical Applications," in "Optical-Thermal Response of Laser-Irradiated Tissue," 2nd ed., A. J. Welch, M. J. C. van Gemert (eds.) Springer Science+Business Media, Dordrecht, Netherlands (2011).
3. S. -K. Kang, R. K. Murphy, S. W. Hwang, S. M. Lee, D. V. Harburg, N. A. Krueger, J. Shin, P. Gamble, H. Cheng, S. Yu, Z. Liu, J. G. McCall, M. Stephen, H. Ying, J. Kim, G. Park, R. C. Webb, C. H. Lee, S. Chung, D. S. Wie, A. D. Gujar, B. Vemulapalli, A. H. Kim, K. M. Lee, J. Cheng, Y. Huang, S. H. Lee, P. V. Braun, W. Z. Ray, and J. A. Rogers, "Bioresorbable silicon electronic sensors for the brain," Nature 530, 71 (2016).
4. M. Choi, M. Humar, S. Kim, and S. H. Yun, "Step-index optical fiber made of biocompatible hydrogels," Adv. Mater. 27, 4081 (2015).
5. K. H. Tow, D. M. Chow, F. Vollrath, I. Dicaire, T. Gheysens, and L. Thévenaz, "Spider silk: a novel optical fibre for biochemical sensing," Proc. SPIE 9634, 96347D (2015).
6. J. Guo, X. Liu, N. Jiang, A.K. Yetisen, H. Yuk, C. Yang, A. Khademhosseini, X. Zhao, and S. H Yun, "Highly Stretchable, Strain Sensing Hydrogel Optical Fibers," Adv. Mater. 28, 10244 (2016).
7. D. Shan, C. Zhang, S. Kalaba, N. Mehta, G. B. Kim, Z. Liu, and J. Yang, "Flexible biodegradable citrate-based polymeric step-index optical fiber," Biomaterials 143, 142 (2017).
8. N. Sharmin, A. J. Parsons, C. D. Rudd, and I. Ahmed, "Effect of boron oxide addition on fibre drawing, mechanical properties and dissolution behaviour of phosphate-based glass fibres with fixed 40, 45 and 50 mol% P_2O_5," J. Biomater. Appl. 29, 639 (2014).
9. E. Ceci-Ginistrelli, D. Pugliese, N. G. Boetti, G. Novajra, A. Ambrosone, J. Lousteau, C. Vitale-Brovarone, S. Abrate, and D. Milanese, "Novel biocompatible and resorbable UV-transparent phosphate glass based optical fiber," Opt. Mater. Express 6, 2040 (2016).
10. A. Othonos and K. Kalli, *Fiber Bragg gratings: fundamentals and applications in telecommunications and sensing*. Boston, Mass.; London: Artech House, 1999.
11. F. Berghmans, T. Geernaert, T. Baghdasaryan, and H. Thienpont, "Challenges in the fabrication of fibre Bragg gratings in silica and polymer microstructured optical fibres," Laser Photonics Rev. 8, 27 (2014).
12. C. R. Dennison, P. M. Wild, D. R. Wilson, and M. K. Gilbart, "An in-fiber Bragg grating sensor for contact force and stress measurements in articular joints," Meas. Sci. Technol. 21, 115803 (2010).
13. A. Candiani, M. Konstantaki, A. Pamvouxoglou, and S. Pissadakis, "A shear sensing pad, based on ferrofluidic actuation in a microstructured optical fiber," IEEE J. Sel. Top. Quantum Electron. 23, 5600307 (2016).
14. A. Bertucci, A. Manicardi, A. Candiani, S. Giannetti, A. Cucinotta, G. Spoto, M. Konstantaki, S. Pissadakis, S. Selleri, and R. Corradini, "Detection of unamplified genomic DNA by a PNA-based microstructured optical fiber (MOF) Bragg-grating optofluidic system," Biosens. Bioelectron. 63, 248 (2015).
15. L. Carvalho, N. J. Alberto, P. S. Gomes, R. N. Nogueira, J. L. Pinto, and M. H. Fernandes, "In the trail of a new bio-sensor for measuring strain in bone: osteoblastic biocompatibility," Biosens. Bioelectron. 26, 4046 (2011).
16. J. Albert, A. Schülzgen, V. L. Temyanko, S. Honkanen, and N. Peyghambarian, "Strong Bragg gratings in phosphate glass single mode fiber," Appl. Phys. Lett. 89, 101127 (2006).
17. J. Canning, M. G. Sceats, H. G. Inglis, and P. Hill, "Transient and permanent gratings in phosphosilicate optical fibers produced by the flash condensation technique," Opt. Lett. 20, 2189 (1995).
18. L. Xiong, P. Hofmann, A. Schülzgen, N. Peyghambarian, and J. Albert, "Photosensitivity and thermal stability of UV-induced fiber Bragg gratings in phosphate glass fibers," Opt. Mater. Express 4, 1427 (2014).

19. M. Choi, J. W. Choi, S. Kim, S. Nizamoglu, S. K. Hahn, and S. H. Yun, "Light-guiding hydrogels for cell-based sensing and optogenetic synthesis in vivo," Nat. Photonics 7, 987 (2013).
20. S. J. Hewlett, J. D. Love, G. Meltz, T. J. Bailey, and W. W. Morey, "Cladding-mode coupling characteristics of Bragg gratings in depressed-cladding fibre," Electron. Lett. 31, 820 (1995).
21. J. Albert, L. -Y. Shao, and C. Caucheteur, "Tilted fiber Bragg grating sensors," Laser Photonics Rev. 7, 83 (2013).
22. T. Poulsen, M. O. Berendt, A. Bjarklev, L. Grüner-Nielsen, and C.E. Soccolich, "Bragg grating induced cladding mode coupling caused by ultra-violet light absorption," Electron. Lett. 34, 1007 (1998).
23. C. -F. Chan, C. Chen, A. Jafari, A. Laronche, D. J. Thomson, and J. Albert, "Optical fiber refractometer using narrowband cladding-mode resonance shifts," Appl. Opt. 46, 1142 (2007).
24. S. Pissadakis and C. Pappas, "Planar periodic structures fabricated in Er/Yb-codoped phosphate glass using multi-beam ultraviolet laser holography," Opt. Express 15, 4296 (2007).
25. S. Pissadakis, M. Livitziis, and G. D. Tsibidis "Investigations on the Bragg grating recording in all-silica, standard and microstructured optical fibers using 248 nm 5 ps, laser radiation," J. Eur. Opt. Soc. - Rapid Publ. 4, 09049 (2009).
26. S. Yliniemi, S. Honkanen, A. Ianoul, A. Laronche, and J. Albert, "Photosensitivity and volume gratings in phosphate glasses for rare-earth-doped ion-exchanged optical waveguide lasers," J. Opt. Soc. Am. B 23, 2470 (2006).
27. M. Sozzi, A. Rahman, and S. Pissadakis, "Non-monotonous refractive index changes recorded in a phosphate glass optical fibre using 248nm, 500fs laser radiation," Opt. Mater. Express 1, 121 (2011).
28. R. K. Brow, "Review: the structure of simple phosphate glasses," J. Non-Cryst. Solids 263&264, 1 (2000).
29. D. Palles, I. Konidakis, C. P. E. Varsamis, and E. I. Kamitsos, "Vibrational spectroscopic and bond valence study of structure and bonding in Al_2O_3-containing AgI–$AgPO_3$ glasses," RSC Adv. 6, 16697 (2016).
30. T. I. Suratwala, R. A. Steele, G. D. Wilke, J. H., Campbell, and K. Takeuchi, "Effects of OH content, water vapor pressure, and temperature on sub-critical crack growth in phosphate glass," J. Non-Cryst. Solids 263&264, 213 (2000).
31. R. Gassino, Y. Liu, M. Konstantaki, A. Vallan, S. Pissadakis, and G. Perrone, "A fiber optic probe for tumor laser ablation with integrated temperature measurement capability," J. Lightwave Technol. 35, 3447 (2017).